Hydrogen solubility in pure iron and effects of alloying elements on the solubility in the temperature range 20 to 500° C

W. Y. CHOO, JAI YOUNG LEE, C. G. CHO
The Korea Advanced Institute of Science, PO Box 150 Chongyangi, Seoul, Korea

S. H. HWANG
Korea Institute of Science and Technology, PO Box 131, Dong Dae Moon, Seoul, Korea

Hydrogen solubility in pure iron and iron based binary alloys have been measured in the temperature range 20 to 500° C under hydrogen at atmospheric pressure. For pure iron, hydrogen solubility decreases as the temperature decreases until about 300° C and then increases reaching maximum at 80° C. The maximum solubility at this temperature was about 0.9 ppm. This large value is thought to result from chemisorption of hydrogen at the grain boundary. The addition of alloying elements, Mo, W and Ni increased the temperature at which hydrogen solubility had its maximum and had no other effects on the trend of hydrogen solubility change as a function of temperature for pure iron. The higher heats of chemisorption of hydrogen onto Mo and W compared with Fe may be responsible for the change in temperatures. Other possible methods of trapping hydrogen in iron and iron based binary alloys are discussed.

1. Introduction

It is well known that hydrogen has a drastic effect on the mechanical properties of iron. The iron–hydrogen system is also important, both from the point of view of the thermodynamic and from the kinetic studies of the interstitial solid solutions. In spite of the large extent of the research work on hydrogen behaviour in the iron–hydrogen system, a large degree of uncertainty and confusion still remains due to its complex nature in the low temperature range. Darken and Smith [1] discovered that the amount of hydrogen absorbed in cold-worked steel from acid solution at room temperature is many times greater than that absorbed in hot-worked steel. They suggested that many lattice defects were produced by cold working and hydrogen trapped in these lattice defects. So the amount of dissolved hydrogen in iron increases by cold working.

After this suggestion, there were many investigations on the trap nature of the hydrogen dissolution mechanism. Suggested trap sites are microvoid [2, 3], dislocation [4, 5], stacking fault [6], two-phase boundary [7], grain boundary, etc. But many different trapping mechanisms and types of trap sites are suggested by different researchers.

There are some investigations about the effect of alloying elements on hydrogen solubility in liquid iron [8], but there are few works available on solid iron. The effect of alloying elements on hydrogen solubility may be very different between liquid iron and solid iron because of the periodic nature of the lattice and strain energies involved in solid iron.

The purpose of this work is to determine the solubility of hydrogen in pure α-iron and to observe the effect of the alloying elements, such as Mo, W, Ni and Cr on the hydrogen solubility in iron. Dominant trap sites and the effects of alloying elements on the trapping mechanism are discussed and a trap model is suggested from the experimental results.

TABLE I Impurities of alloying elements and pure ESPI iron*

Element	Fe	Ni	Cr	Mo	Si	C	O	Ag	Mn
Pure Fe[†]	5N	2	–	–	1	–	–	1	3
Ni[†]	2	4N5	–	–	1	–	–	1	–
Mo[†]	10	–	10	3N5	–	10	280	–	–
Electrolytic iron	3N5	–	–	–	50	50	–	–	50
Cr	–	–	4N	–	–	–	–	–	–

*Impurities of pure iron, electrolytic iron and alloying elements, in ppm by weight. 5N: 99.999%, 4N: 99.99%, 3N5: 99.95% and 4N5: 99.995%.
[†]Purchased from ESPI.

2. Experimental procedure

The specimen of pure iron employed in this work was a 99.999% pure iron rod obtained from ESPI*. Other specimens with alloying elements, were made in an induction furnace under vacuum, adding the required amount of alloying element to electrolytic iron to be within the α-range. The amount of impurities of pure ESPI iron and alloying elements used are given in Table I. The final compositions of the alloyed specimens manufactured in the laboratory are given in Table II.

The alloyed ingots were annealed for 48 h at 1100°C to homogenize and then were cut to pieces of about 1 g weight, each in a cylindrical shape. Pure iron and alloyed specimens were vacuum annealed for 1.5 h at 900°C to extract the residual hydrogen which may be strongly bound [3, 9] in the samples. The vacuum annealed specimens were charged with hydrogen in the temperature range 25 to 500°C at 1 atm H_2 pressure and quenched in liquid nitrogen using the apparatus shown in Fig. 1. Hydrogen was charged for 3 h at the specified temperature. The contact time, 3 h was tabulated to reach constant hydrogen concentration throughout the specimen when the hydrogen had a diffusivity of $10^{-6} cm^2 sec^{-1}$ in α-iron. Hydrogen, 99.999% purity, from Matheson Co., was used for the above procedure. The amount of hydrogen in the specimen was analysed by hot vacuum extraction apparatus with 0.1 ppm sensitivity (Loco Hydrogen Analyser). Since the adsorbed hydrogen at the external surface of the specimen could not be removed experimentally, the amount of adsorbed hydrogen calculated was substrated from the experimental values. The density of the specimen was also measured to determine the amount of microvoid present.

3. Results and discussions
3.1. Hydrogen solubility in pure iron
Geller and Sun [9] have measured hydrogen solubility in pure iron above 400°C and reported the solubility as a function of temperature under an atmospheric pressure of hydrogen.

$$C(ppm) = 42.7 \exp(-6500(cal)/RT) \quad (1)$$

where C is solubility, R the gas constant and T is absolute temperature. Equation 1 represents lattice solubility of hydrogen in pure iron because the trapping effect generally starts to show below 300°C. Fig. 2 shows hydrogen solubility in pure iron plotted against the reciprocal of temperature at one atmosphere. It was found that this result agrees well with Geller and Sun's in the temperature range 300 to 500°C. However, below 300°C an abnormally high solubility was observed, quite different from that found when testing the data of Geller and Sun. Another distinct feature is that solubility shows a maximum value in the temperature range 80 to 140°C when the hydrogen concentration is 0.9 ppm. This value is much higher than the lattice solubility of 0.006 ppm obtained from Equation 1 at this temperature. So one can conclude that most of the hydrogen in this range exists in trapping sites.

At this point, it is appropriate to review suggested trapping sites and trapping mechanisms carefully reflecting the results shown in Fig. 2.

TABLE II Compositions of alloyed specimens.

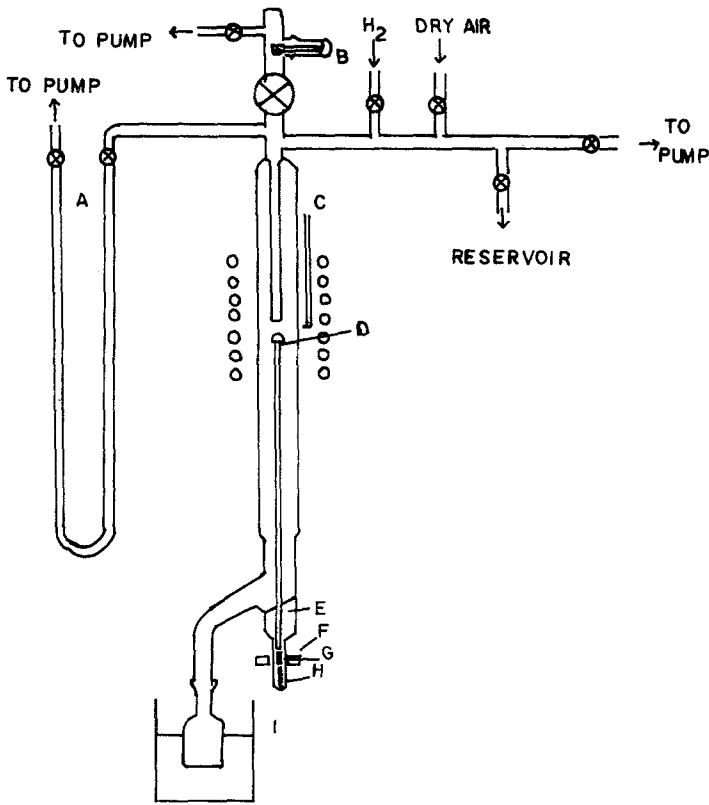| Composition	Fe–Mo	Fe–W	Fe–Cr	Fe–Ni
Alloying element	Mo	W	Cr	Ni
Wt % of	1.8	0.8	1.0	1.5
alloying element	2.6	2.48	2.0	2.2
	3.35	3.8	3.0	3.2
	–	4.3	–	–

*Electronic Space Products Inc.

Figure 1 Schematic diagram of hydrogen charging apparatus (A) mercury manometer (B) specimen dropper (C) thermocouple (D) specimen holder (E) aluminum (F) magnet (G) steel rod (H) spring and (I) liquid nitrogen.

3.1.1. Hydrogen trapping in dislocations

Since, as stated in the experimental procedure, the iron specimens used were fully annealed, one can assume that the dislocation density in the specimen was 10^8 lines cm^{-2}. Assuming one H atom is trapped per Fe atom in the dislocation core, the number of trapped hydrogen atoms is 2.5×10^{15}, or 0.01 ppm. This value is about one hundred times smaller than the peak value of hydrogen solubility in Fig. 2. The problem arises from the assumption of one H atom per Fe atom in the dislocation core. However, results of recent researches [10, 11] do not accept 100 H atoms per Fe atom in the dislocation core. From this one can conclude that trapping in the dislocation core does not effect the solubility of hydrogen in this range.

Figure 2 Temperature dependence of hydrogen solubility in pure iron at 1 atm pressure.
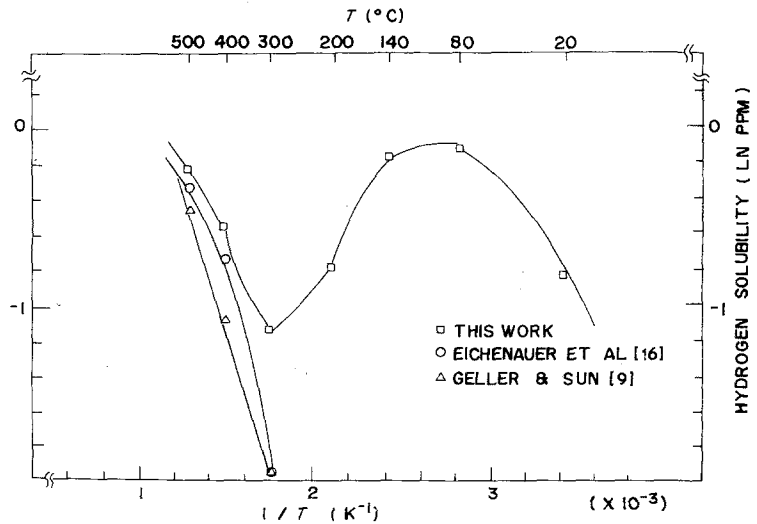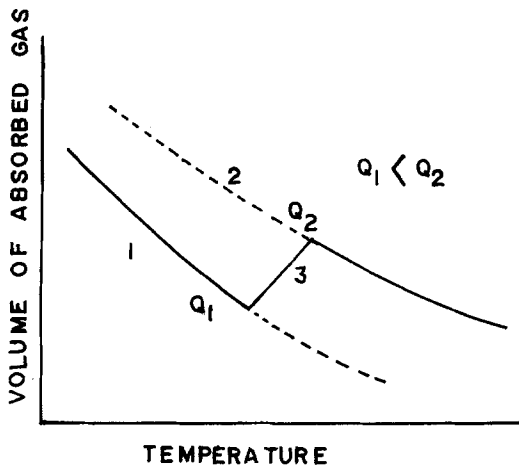
Figure 3 General mode of transition between physical and chemical adsorption (1) physical adsorption (2) chemical adsorption (3) transition range (Q_1) heat of physical adsorption and (Q_2) heat of chemical adsorption.

3.1.2. Hydrogen trapping in microvoids

The density of a fully annealed specimen was measured to check the amount of microvoid present. The measured density was very close to the theoretical density of pure iron $7.87 \, \mathrm{g \, cm^{-3}}$ within experimental error. Therefore the amount of microvoid present is disregarded as a possible trapping site in this case.

3.1.3. Hydrogen absorption on the surface

Fig. 3 shows the amount of adsorbed gas on the metal surface against temperature as given by Taylor [12]. As the temperature increases the nature of the adsorption phenomenon changes from physical adsorption to chemical, and at the transition point, a maximum value of adsorption appears. The trend of adsorption shown in Fig. 3

is very similar to our results, which draws our attention to this behaviour. The surface area of the specimen is $1.5 \, \mathrm{cm^2}$. Considering a roughness factor of the surface of 1.6, the actual area was $2.4 \, \mathrm{cm^2}$. Under the assumption that hydrogen forms a monomolecular layer on the whole surface of specimen, the specimen held 3.4×10^{15} hydrogen atoms, or 0.015 ppm. This value which is the maximum value obtained from surface adsorption is too small to explain our experimental value, so it is disregarded as a possible trap mechanism.

3.1.4. Hydrogen trapping in the grain boundary

Werner and Davis [13] found a maximum solubility of hydrogen at $250^{\circ} \mathrm{C}$ in cold-rolled iron, and they explained the phenomenon as being due to chemisorption of hydrogen in the lattice defects of iron. Werner and Davis' work suggests chemisorption in the grain boundary as a possible trapping mechanism. Fig. 4 shows grain boundary structures, (a) represents the microstructure of pure iron rod as-received while (b), the microstructure of sample specimen after the whole experimental procedure, shows grain growth and the subgrain boundary developed during the experiments. The area of the grain boundary including the subgrain boundary was measured under the microscope and found to be $160 \, \mathrm{cm^2 \, g^{-1}}$ Fe. In order to calculate the number of hydrogen atoms chemisorbed in the grain boundary the following assumptions have been made:

(1) The characteristic values of the chemisorption of hydrogen in the grain boundaries, θ, Q and E_a were assumed to be the same as those on the surface, since no data were available for hydrogen chemisorption in grain boundaries.
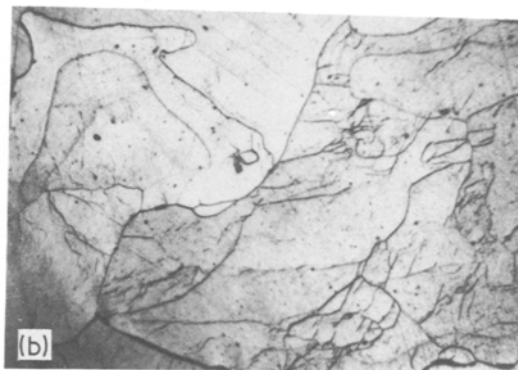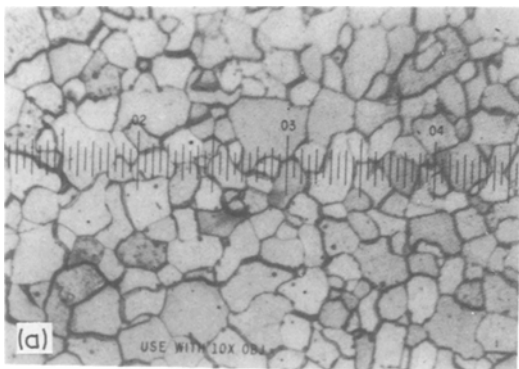

Figure 4 Microstructure of the pure iron (a) before vacuum annealing and (b) after annealing, hydrogen charging and analysing ($\times 76$).

(2) The area occupied by one Fe atom in the lattice site and in the grain boundary is the same.

(3) One hydrogen atom is absorbed onto one Fe atom and the grain boundary is fully covered by hydrogen atoms.

With the above assumptions and assuming that the grain boundary has two sides with are capable of hydrogen chemisorption, the number of hydrogen atoms chemisorbed at the grain boundary is 4×10^{17}, or 1.6 ppm. If it is assumed that the coverage of hydrogen in grain boundary (θ) is 0.6, the trapped hydrogen in the grain boundary will be 0.9 ppm.

If one could prove that the peak value occurs at 80 to 140° C under the above conditions, the mechanism of hydrogen trapping at the grain boundary is reasonable. T_A, at which maximum hydrogen solubilibly is observed will be estimated by utilizing adsorption theory.

Adamson [14] derived equations for gas adsorption on metals by assuming that the rate is proportional to the number of gas molecules colliding on the surface and at active sites; and for desorption rate, proportional to the vibration frequency of gas adsorbed and the number of adsorbed sites on the surface, respectively, as given in Equations 2 and 3.

$$R_a = \frac{d\theta}{dt} = \frac{N\sigma_0}{(2\pi MRT)^{1/2}} P(1-\theta)^2 \exp(-E_a/RT) \quad (2)$$

where R_a is adsorption rate, N is Avogadro's number, σ_0 is area per trap site, P is hydrogen pressure, E_a is activation energy of chemisorption at the grain boundary, R is the gas constant, T is absolute temperature, M is molecular weight of hydrogen and t is time of the experiment.

$$R_d = \frac{1}{\tau_0}\theta^2 \exp(-Q/RT)\exp(-E_a/RT) \quad (3)$$

where R_d is desorption rate, τ_0 is mean stay time of gas atom and Q is heat of chemisorption at the grain boundary.

From the adsorption characteristics shown in Fig. 3 one can assume that grain boundary coverage (θ) is dependent only on adsorption rate because the system does not reach equilibrium at $T < T_A$. The amount of hydrogen chemisorbed at time t can be rewritten as Equation 4 by integrating Equation 2.

$$\theta = \frac{\beta t}{1 + \beta t} \quad (4)$$

where

$$\beta = \frac{N\sigma_0}{(2\pi MRT)^{1/2}} P \exp(-E_a/RT).$$

If $T > T_A$, the system attains equilibrium.

$$R_a = R_d. \quad (5)$$

Equating Equations 2 and 3, Equation 6 is obtained

$$\theta = \frac{\alpha}{1 + \alpha} \quad (6)$$

where

$$\alpha = \left[\frac{N\sigma_0 P}{(2\pi MRT)^{1/2}}\right]^{1/2} \tau_0^{1/2} \exp(Q/2RT).$$

Since the grain boundary coverage (θ) should be the same at T_A in Equations 4 and 6, the following relation is established

$$\beta t = \alpha. \quad (7)$$

Substituting α and β into Equation 7, Equation 8 is derived

$$T_A^{1/4} \exp(Q/2RT + E_a/RT) \\ = \left[\frac{N\sigma_0 P}{(2\pi MR)^{1/2}}\right]^{1/2} t/\tau_0^{1/2}. \quad (8)$$

θ is already obtained from our data ($\theta = 0.6$) but E_a can not be obtained from data available in the literature. Accepting Adamson's [14] assumption, $Q/2 + E_a \simeq Q^*/2$ at $\theta = 0.6$ where Q^* is the heat of chemisorption at the grain boundary in the case of $\theta = 0$, Equation 8 becomes Equation 9

$$T_A^{1/4} \exp(Q^*/2RT) = \left[\frac{N\sigma_0 P}{(2\pi MR)^{1/2}}\right]^{1/2} t/\tau_0^{1/2}. \quad (9)$$

Bikerman [15] compiled data of heat of chemisorption of hydrogen (Q^*) on various metal surfaces as shown in Table III. For iron, the heat of chemisorption is $34 \, \text{kcal mol}^{-1}$. As the heat of chemisorption in the grain boundary is assumed to

TABLE III The heat of chemisorption of hydrogen Q^* ($\theta \to 0$) on a clean metal surface.

Metal	$Q(\text{kcal mol}^{-1})$
Fe	32,36,34
Cr	45(24)*
W	45(46)
Mo	40(43)
Ni	31(29)

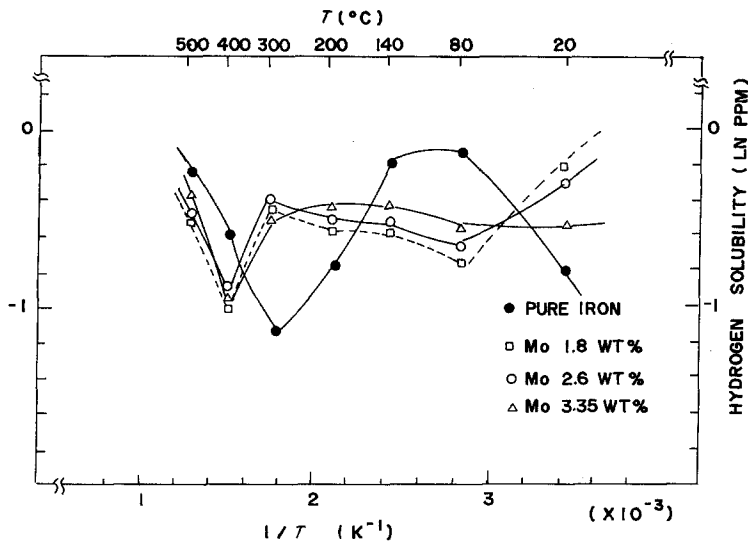*Values in parentheses are calculated from Pauling's equation.

Figure 5 Temperature dependence of hydrogen solubility in α-Fe adding Mo at 1 atm H_2 pressure.

be the same as that of surfaces, substituting this value into Equation 9 gives $T_A = 80°C$. This agrees very well, with our experimental data which show maximum hydrogen solubility at $80°C$.

Although many assumptions are involved in developing a relation for T_A, the chemical adsorption of hydrogen in the grain boundary can explain the abnormal behaviour of hydrogen solubility below $300°C$.

3.2. The effects of alloying elements on hydrogen solubility in iron

Figs 5 to 8 are hydrogen solubility against $1/T$ plots for Fe—Mo, Fe—W Fe—Cr and Fe—Ni alloys, respectively.

In Figs 5 and 6, the T_A and T_B increase as alloy-ing elements Mo and W are added to the iron. T_A is the temperature at which maximum hydrogen solubility is observed, and T_B is the temperature at which the trapping effect begins. Equation 9 indicates that if Q^* increases T_A should increase. From Table III, one finds that the heats of chemisorption of Mo and W are much higher than that of pure iron, resulting in higher T_A and T_B values for these cases. The peak values of hydrogen solubility should be proportional to the grain boundary area as suggested above. Fig. 9a and b shows microstructures of Fe—2.6 wt%W and Fe—3.8 wt%W, respectively. The area of the grain boundary is $100 \, cm^2 \, g^{-1}$—Fe which is far less than that of pure iron, $160 \, cm^2 \, g^{-1}$—Fe. This explains well the relatively low hydrogen solubility for these alloy

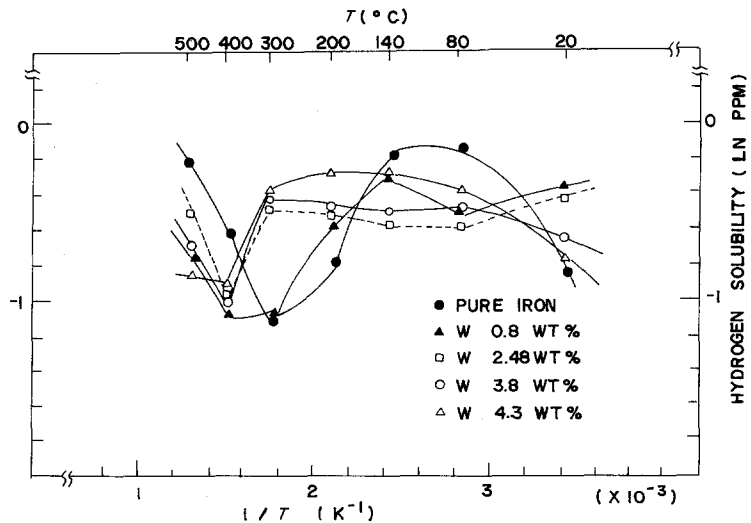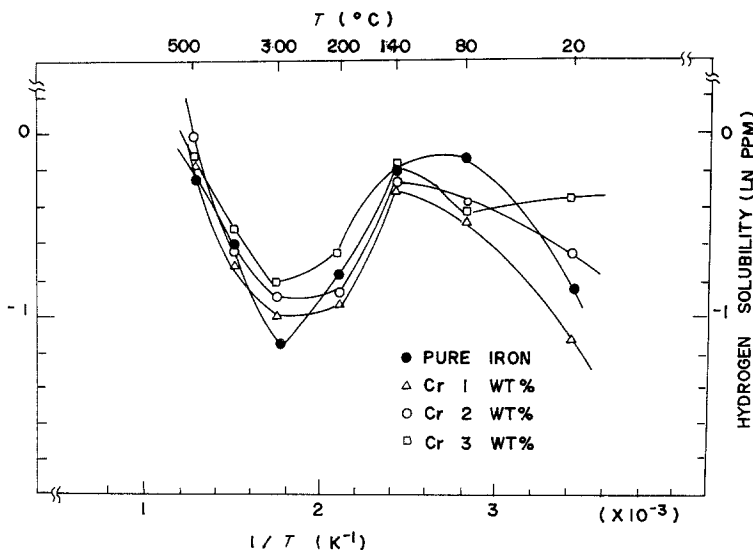*Figure 6* Temperature dependence of hydrogen solubility in α-Fe adding W at 1 atm H_2 pressure.

systems compared to that of pure iron. T_A and T_B for Fe–Cr alloys are very similar to those for pure iron as shown in Fig. 7 except that the maximum value is slightly lower. The heat of chemisorption for Cr of 45 kcal mol^{-1} and 24 kcal mol^{-1} are reported (see Table III).

If the medium value is taken, one may think that this value is very close to that of iron. Again observation of the Fe–Cr system is further support for the hydrogen chemisorption mechanism in the grain boundary.

In Fig. 8 hydrogen solubilities for Fe–Ni alloys are given. T_A and T_B increase while Q^* is less than that for pure iron. For this case the shifts of T_A and T_B cannot be explained by the above argument. However, the low solubility at T_A was due

to small grain boundary area for these alloys. The grain boundary area for Fe–2.2 Wt%Ni alloy in Fig. 9d was about 100 cm^2 g^{-1}–Fe which is much smaller than that of pure iron, 160 cm^2 g^{-1}–Fe.

4. Conclusions

(1) For fully annealed pure iron, hydrogen solubility was measured at 25 to 500° C at atmospheric pressure. The hydrogen trapping phenomenon starts at 300° C (T_A) and the maximum solubility of hydrogen (T_B) is observed at 80° C. The amount of hydrogen was 0.9 ppm. The hydrogen trapping phenomenon is interpreted as hydrogen adsorption in the grain boundary.

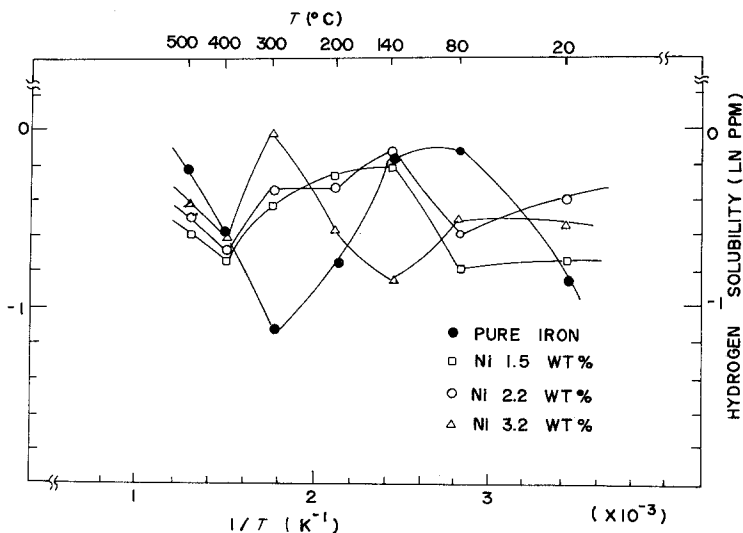(2) Mo, W and Ni increase T_A and T_B while Cr does not change the critical temperatures. These

Figure 8 Temperature dependence of hydrogen solubility in α-Fe adding Ni at 1 atm H₂ pressure.
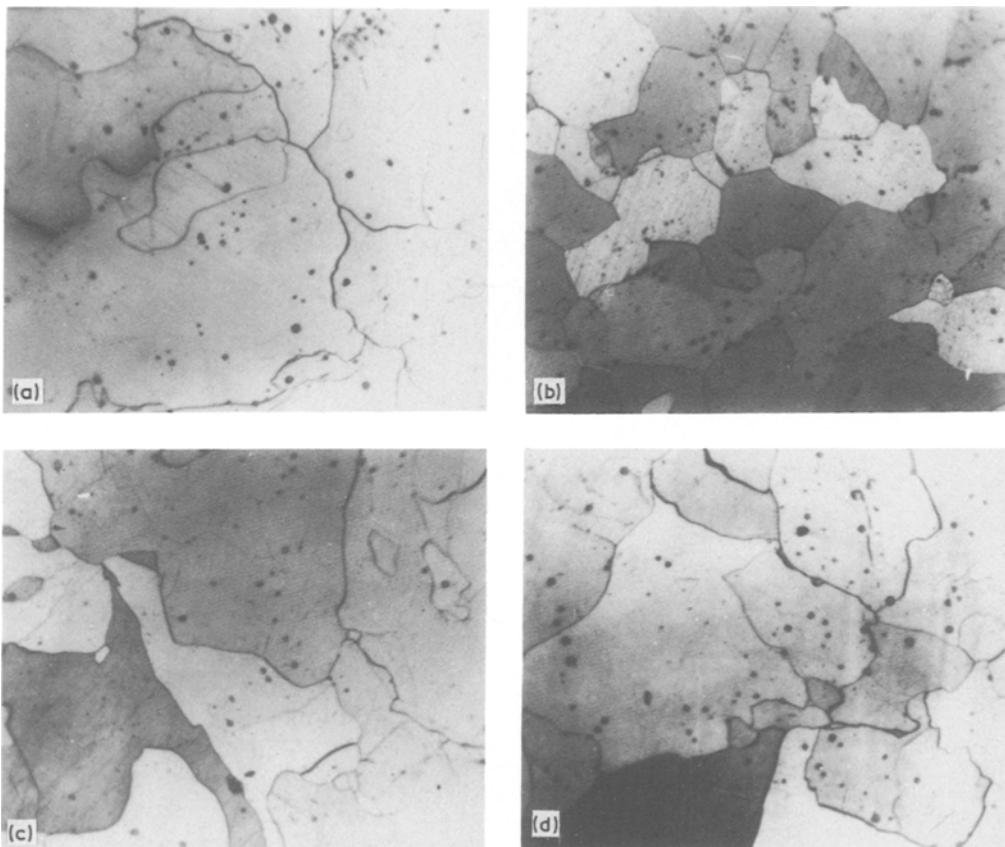
Figure 9 Microstructures of the specimen after vacuum annealing, hydrogen charging and analysing (a) Mo 2.6 wt%–Fe, (b) W 3.8 wt%–Fe, (c) Cr 2.0 wt%–Fe and (d) Ni 2.2 wt%–Fe (× 80).

phenomena, except Ni, can be explained by the change of heat of chemisorption of hydrogen by these elements.

(3) The maximum hydrogen solubility is decreased by adding alloying elements, Mo, W, Ni and Cr. This is discussed through the reduction of the grain boundary area as alloying elements are added.

References

1. L. S. DARKEN and R. P. SMITH, *Corrosion* **5** (1949) 1.
2. D. M. ALLEN-BOOTH and J. HEWITT, *Acta Met.* **22** (1974) 171.
3. M. L. HILL and E. W. JOHNSON, *Trans. AIME* **215** (1959) 717.
4. R. GIBALA, *ibid.* **239** (1967) 1574.
5. R. A. ORIANI, *Acta Met.* **18** (1970) 147.
6. M. A. WHITEMAN and A. R. TRIANO, *Phys. Stat. Sol.* **7** (1964) K109.
7. J. F. NEWMANN and L. L. SHREIR, *J. Iron Steel Inst.* **207** (1969) 1369.
8. J. CHIPMAN, "Basic Open Hearth Steelmaking", (American Institute of Metals and Engineering, New York, 1951) pp. 640–724.
9. W. GELLER and T. H. SUN, *Arch. Eisenhuttenw* **21** (1950) 423.
10. J. P. HIRTH and B. CARNAHAN, *Acta Met.* **26** (1978) 1795.
11. R. A. ORIANI, Proceedings of the Conference on Fundamental Aspects of Stress Cracking, 1967, Columbus, Ohio, National Association of Corrosion Engineers (Stoeh Leed, Houston, 1969) p. 32.
12. H. S. TAYLOR, *J. Amer. Chem. Soc.* **53** (1931). 578.
13. J. E. WERNER and H. M. DAVIS, *Trans. ASM* **53** (1961) 853.
14. A. W. ADAMSON, "Physical Chemistry of Surfaces", (John Wiley and Sons, New York, (1976) pp. 522–62.
15. J. J. BIKERMAN, "Surface Chemistry", (Academic Press, London and New York 1958) pp. 301–67.
16. W. EICHENAUER, H. KUNZIG and A. PEBLER, *Z. Metallk.* **49** (1958) 220.